Theor. Appl. Climatol. 65, 1–15 (2000)

Theoretical and Applied Climatology

[1]Meteorological Institute of the University of Hamburg, Germany
[2]Max-Planck-Institute for Meteorology, Hamburg, Germany

Secular Variability of the Coupled Tropospheric and Stratospheric Circulation in the GCM ECHAM 3/LSG

F. Feser[1], **H.-F. Graf**[2], and **J. Perlwitz**[2]

With 15 Figures

Received February 22, 1999
Revised August 5, 1999

Summary

Secular or multi-decadal variability is a widely observed phenomenon, apparent in instrumental and paleo climatic records. These long time oscillations are found in many variables of the climate system. The ocean especially experiences low frequency variations. But also atmospheric variables such as temperature, wind velocity and sea level pressure can show secular variability.

The low frequency variability here is examined in the coupled atmosphere-ocean model ECHAM3/LSG T21. A coupled stratospheric and tropospheric mode is detected oscillating with a period of approximately 100 years. The atmospheric pressure system mainly involved in this oscillation is the northern hemispheric winter stratospheric polar vortex. The near surface temperature experiences variations of the same magnitude as the observed temperature trends of the last decades. Multi decadal variability is also shown in the North Atlantic Oscillation Index.

A shift of the length of the oscillation period between longer and shorter time scales indicates that chaotic processes might be responsible for the variability.

1. Introduction

The increasing anthropogenic influence on the climate system requires an intensified research also of natural variability modes. A better understanding of these natural oscillations is the basis for an improved estimate of the human impact on the earth and a more accurate climate predictability.

Recently, intensified effort has been made to reveal climate variability on decadal to secular time scales in observational data as well as in general circulation models (GCMs). Historical records of climate variability on multi-decadal time scales are frequently found in proxy data. One example of these non-instrumental data sources are ice cores. A frequently used technique to determine the historical temperature is the analysis of the comparison of the concentration of the oxygen isotope ^{18}O to the oxygen isotope ^{16}O contained in the ice cores and cores from deep sea drillings. Johnson et al. (1970) and Dansgaard et al. (1970) examined ice cores from Camp Century in the northwestern part of Greenland. These records revealed oscillations of periods around of approximately 78 and 181 years. Appenzeller et al. (1998) showed that the inter-annual to decadal fluctuations in western Greenland snow accumulation and net precipitation are correlated with the NAO and can thus be used for the reconstruction of a NAO proxy data time series. The resulting 350 year time series (Appenzeller et al., 1998) is examined using wavelet analysis. The calculations show oscillations with periods ranging from some years to decades (see their Fig. 3). Secular variability occurs since the middle of the 19th century. The shorter periods are evenly distributed over the

entire time series, while the secular variability first shows up after about 200 years. Another important data source are time series reconstructed from tree rings. LaMarche (1974) found variabilities of 70 and 110 years in trees of the White Mountains, Nevada. Stuiver and Braziunas (1989) extracted secular oscillations of approximately 150 and 420 years examining the δ^{14}C concentration in trees. δ^{14}C is constantly formed in the atmosphere by the reaction of nitrogen and neutrons, which are generated by cosmic radiation. By analyzing the δ^{14}C concentration a changed intensity of the cosmic radiation flux forced by solar activity can be detected. Pollen concentrations in sea and lake sediments are another source of proxy data which can document climate regime shifts of the past. Gajewski (1988) shows variations in the range of 95, 125 and 330 years in records of the pollen concentration for the last 2000 years near the Great Lakes and the Atlantic coast with a statistical significance of at least 95%.

Instrumental records are usually too short to reveal secular variability. The 'Central England' temperature record (Manley, 1974; Lamb, 1977; Schönwiese, 1978), being the longest instrumental data record, includes variabilities of 99% statistical significance with periods of about 24 and 100 years. Secular variability is also often detected in coupled atmosphere-ocean models. Delworth et al. (1993) revealed in their coupled ocean-atmosphere model (GFDL, described in detail by Manabe et al. (1991)) an irregular oscillation of the thermohaline circulation in the northern Atlantic at a time scale of 50 years. Tett et al. (1997) show variability in the northwestern Atlantic also with a period of about 50 years in a 1000 year control run of the HADCM2-CTL. Hence, in observations as well as in models, multidecadal variability has been observed for some parameters. Frequencies do not seem to be stable and the reasons for the oscillations, if any, are not well understood.

An internal model oscillation can lead to altered results for climate change scenarios computed with the model. Cubasch et al. (1994) calculated four climate change experiments which differed only in the simulation starting time. This method is known as Monte Carlo simulation. The climate change scenario used was the IPCC scenario A (Houghton et al., 1990). The calculation started in 30 years intervals from a control run of the coupled atmosphere-ocean model ECHAM1/LSG. After 50 simulated years the global mean temperature of the four realizations differed by up to 0.4 K. This example showed the possible effect of an internal control run oscillation on climate change scenarios. Therefore the model's internal vacillation has to be examined in more detail. Even if the variability does not represent a natural variability mode it can still lead to differing results of climate scenario simulations.

In this paper secular climate variability is examined using the atmosphere-ocean model ECHAM3/LSG at T21 resolution. This model was intensively used for climate change assessment studies (Hegerl et al., 1997; Schiller et al., 1996). We use the zonal mean zonal wind as a parameter of the general circulation which can represent the leading fundamental variability mode of the atmosphere (Perlwitz and Graf, 1995). Two regimes are selected, corresponding to states of anomalously strong or weak zonal mean zonal wind in the northern hemisphere polar vortex area, respectively. In order to examine which climate variables are connected with these regimes, composites are calculated for the two zonal wind regimes. Afterwards the role of the deep ocean is investigated. Possible reasons for the identified oscillation will be discussed at the end of the paper.

2. Model and Experiment Description

The model used in this paper for a closer examination of secular climate variability is the coupled atmosphere-ocean model ECHAM3/LSG.

The atmosphere model ECHAM3 has been changed for climate simulation purposes. These changes include new parameterizations of clouds, horizontal diffusion, radiative processes and changes of the planetary boundary layer. The model physics are described by Roeckner et al. (1992). The primitive equations are the basis of the spectral model ECHAM3. For this work a triangular truncation at the wave number 21 is used. This corresponds to a horizontal resolution of $5.6^\circ \times 5.6^\circ$. The model is divided into 19 atmosphere layers, ranging from 1000 to 10 hPa and a hybrid pressure-sigma coordinate system is

used. The ECHAM3 stratospheric and upper tropospheric part is assumed to be trustworthy because Graf et al. (1997) demonstrate that the stratospheric part of the coupled baroclinic and barotropic coupled modes (Perlwitz et al., n.d.) found by Perlwitz and Graf (1995) is represented well. The LSG (Large Scale Geostrophic) model (Maier-Reimer et al., 1993) is a 3-dimensional global ocean model. It is based on the continuity equations of mass, momentum and energy, the salt concentration and the thermodynamic energy equation. The model's ground topography resolution is $5^\circ \times 2.5^\circ$. A thermodynamic sea-ice model is included. There are 11 vertical layers, ranging from 25 m to 5000 m depths. A more detailed description of the ECHAM3 model can be found in Deutsches Klimarechenzentrum (1994) and the LSG model is specified in Deutsches Kilmarechenzentrum (1992).

The control run used in this paper is described by Voss et al. (1998). The control run contains the constant CO_2 concentration of the year 1985. For our calculations of secular variability a stable 550 year segment of the control run's first PC of zonal mean zonal wind (method is described in chapter 4) from year 350 to year 900 is selected. The first 350 years are omitted because the model experiences spin up problems. After the year 900 a shift towards shorter amplitudes and shorter frequencies can be detected. This feature of the model is discussed in chapter 6. Our analysis is based on winter means, this way high frequency noise is filtered out.

3. Observed Trends

During winter a coupled mode of stratospheric and tropospheric circulation is the prevailing pattern. This mode describes the connection between the strength of the stratospheric vortex and the tropospheric westerlies over the northern Atlantic (Perlwitz and Graf, 1995).

The observed stratospheric (50 hPa) winter-trends of geopotential height (see Fig. 1a of Perlwitz et al. (1997)) show that the northern hemispheric polar low pressure vortex has strengthened during the last 38 years. A positive trend of 50 hPa geopotential height is apparent over the southern part of Europe and northern Africa. The most prominent feature of the winter trend is the increased pressure gradient between the strong polar vortex and the positive geopotential height anomalies over the temperate latitudes (Kodera and Koide, 1997). This results in a strengthening of the zonal wind especially in the vicinity of the polar vortex (Thompson and Wallace, 1998). In the troposphere (500 hPa) (see Fig. 1b of Perlwitz et al. (1997)) a decrease of geopotential height at the 500 hPa-level appears during the last three decades south of Greenland. Together with positive geopotential height trends over the Mediterranean Sea and North Africa a strengthened NAO-index results.

Motivated by the question whether the observed winter trends of geopotential height are caused by natural climate variability or by anthropogenic influence, Perlwitz et al. (1997) calculated a pattern correlation between observed winter geopotential height trends at 500 and at 50 hPa and winter geopotential height trends of the control run of ECHAM3/LSG. Thus, 40-year-long modeled winter trends were examined for conformity with the observed trends between 1957/58 and 1995/96.

The pattern correlation time series (Fig. 1) reveals inter-decadal variability between years of

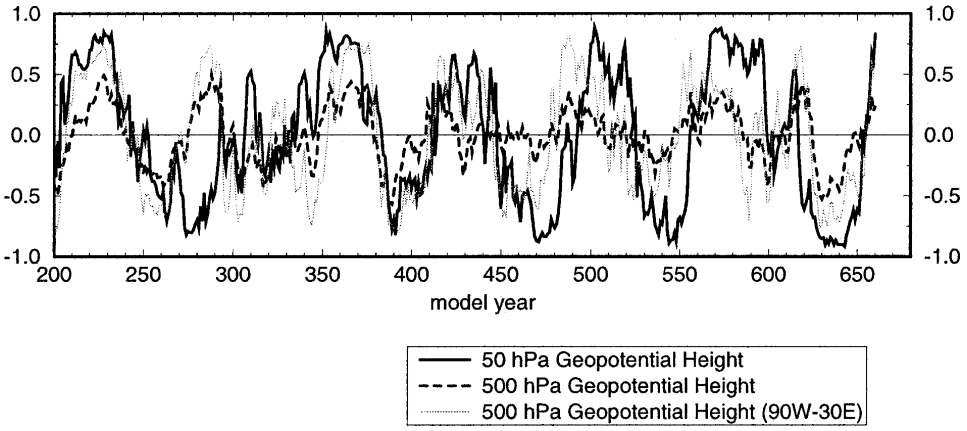

Fig. 1. Time series of pattern correlation between observed winterly geopotential height trends in the stratosphere and in the troposphere (1957/58–1995/96) and 40-year-long modeled geopotential height trends (Perlwitz et al., 1997; Graf et al., 1998)

high pattern conformity and years of negative correlation. Variability is apparent both in the stratosphere and in the troposphere. Most wave activity and baroclinic disturbances are forced in the troposphere and therefore larger correlation coefficients occur in the stratospheric correlation analysis. In the troposphere higher correlation coefficients can be seen for the northern Atlantic region (fine dotted line). During winter months the strength of the westerlies over the northern Atlantic is connected to the strength of the stratospheric polar night jet (Perlwitz and Graf, 1995). This implies a connection between the stratospheric vortex and the North Atlantic Oscillation and higher conformity between the time series of the stratosphere and the troposphere for the northern Atlantic region results. The period of the multi-decadal variability vacillates between approximately 70 and 100 years. The correlation of 38-year-long observed trends and 40-year-long modeled trends implies a possible prevailing of the same trend for 60 to 70 years before it switches sign. During winter the zonal mean zonal wind is a good parameter to show the connection between tropospheric and stratospheric circulation (Kodera et al., 1991; Nigam, 1990; Perlwitz and Graf, 1995). Therefore it is studied more closely in order to get a better qualitative understanding of the inter-decadal variability apparent in the model.

4. Zonal Wind

An Empirical Orthogonal Function (EOF) analysis, based on the covariance matrix, of the zonal mean zonal wind shows the prevailing statistical patterns and their temporal evolution. For this calculation years 350 to 900 of the ECHAM3/LSG control run (Voss et al., 1998) were chosen and a region of the northern hemisphere has been selected from 20° N to 85.76° N. The explained variance of the first EOF of zonal mean zonal wind is 40.5% and 23.3% for the second EOF. The remaining EOFs explain less than 10% of total variance each. The mean anomaly pattern of the first EOF (Fig. 2a, meridional cross-section from 1000 hPa up to 30 hPa) shows the lower part of the stratospheric Polar Night Jet (PNJ) and the Subtropical Jet (STJ). A negative correlation between these two jets can be seen: a weak STJ goes along with a strong PNJ. A relationship between the PNJ and the STJ in observational data has been reported by Kodera et al. (1991). They calculated lagged correlations between the time coefficients of the first loading vector (Nigam, 1990) of the zonal mean zonal wind during the northern hemisphere winter and the zonal mean zonal wind at each grid point. They found a propagation of perturbations in zonal mean zonal wind from the stratosphere to the troposphere. The second EOF (Fig. 2b) shows the PNJ and a relation between

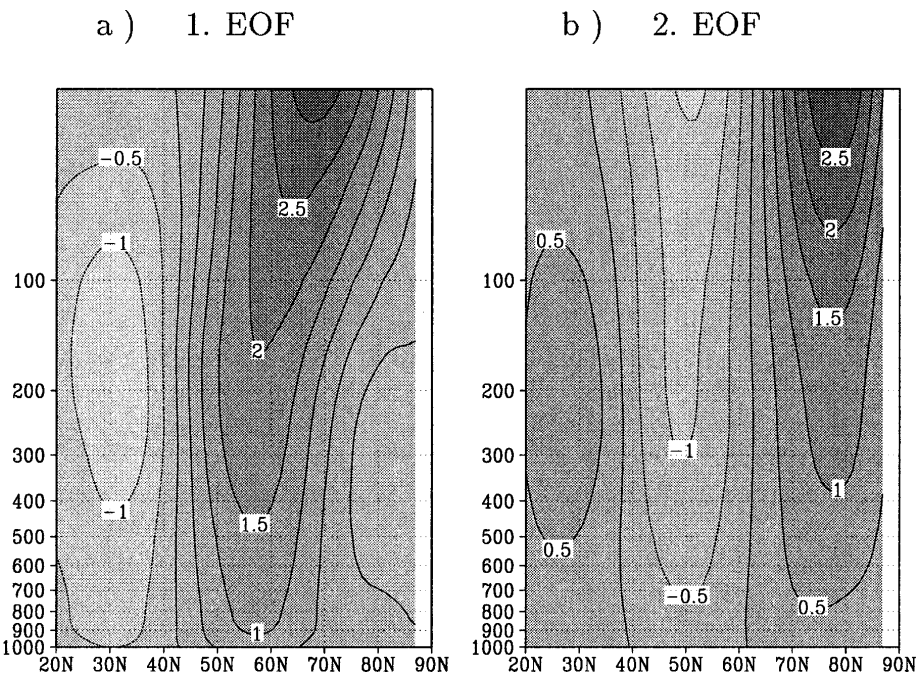

Fig. 2. Meridional cross-sections of the first two EOFs mean anomalies pattern of winterly northern hemisphere (20° N–85.76° N) zonal mean zonal wind measured in m/s

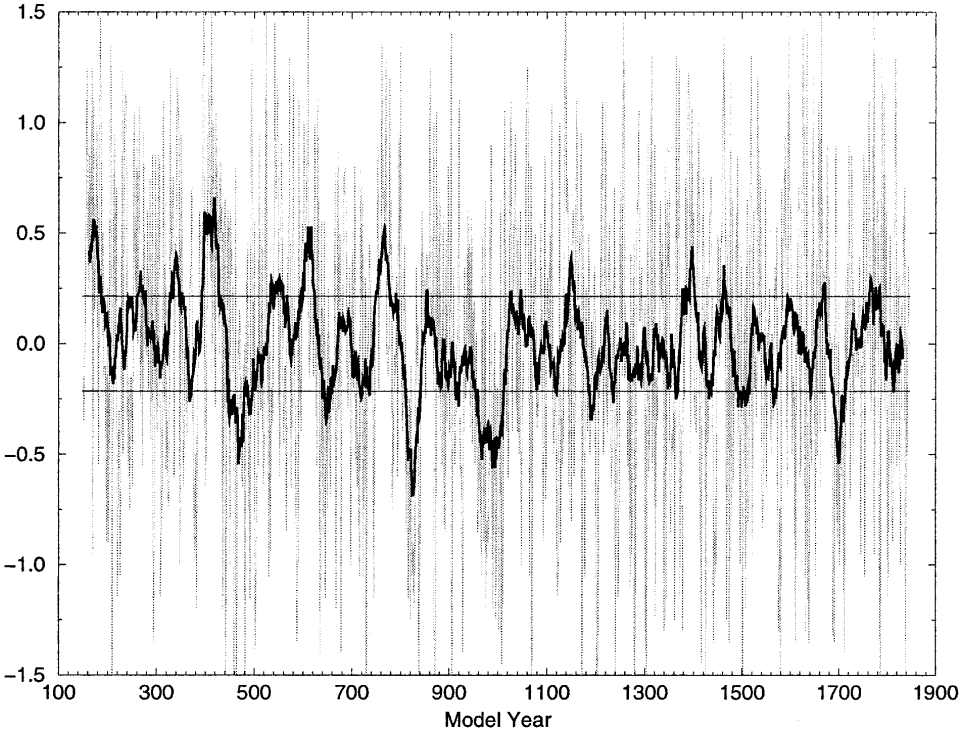

Fig. 3. First principal component of northern hemisphere (20° N–85.76° N) winterly zonal mean zonal wind of the 1848 year control run, smoothed with a two year running mean filter (grey line) and smoothed with a 30 year running average (black line). Horizontal lines indicate one positive and one negative standard deviation of the smoothed time series, respectively

the PNJ and the middle latitude stratospheric wind. The PNJ is concentrated at high latitudes and weak middle latitude winds appear at the same time. This is a pattern of a meridional shift of the polar vortex. If the vortex is strong, it is more concentrated in high latitudes.

The northern hemispheric winter ($\overline{DJF}$) first Principal Component (PC) of the zonal mean zonal wind time series (Fig. 3) reveals an irregular low frequency oscillation. The time series was smoothed using a 30 year running average (thick line) and, in order to extract a strong biannual variation, also with a two year running average (grey lines). For better understanding the reasons for our selection of years 350 to 900 for further calculations the time series is plotted completely. Large amplitudes of the low pass filtered time series can be seen during the three decades around the year 400 and 500 and, at the 30 year means, 750 and 850. There are also sequences of smaller amplitudes in between where the low frequency variability is smaller. For the first 1000 years a multi-decadal to secular oscillation can be seen. Then a shift towards smaller amplitudes and shorter periods occurs.

The first PC zonal mean zonal wind power spectrum (Fig. 4) of the two year running mean filtered time series (years 350 to 900) reveals statistically significant variability at the multi-decadal time scale with a period ranging from 80 to about 200 years. The spectrum was calculated using a Parzen window. This calculation was performed using a time series with each point representing two year means. This excludes a large short period amplitude around two years. This biannual oscillation of the ECHAM3/LSG control run has not been studied in detail so far and it is of no further interest for the current examination of secular variability. The 95% confidence limits based on a red noise spectrum, which would have been generated by a first-order autoregressive process, is displayed. The low frequency peak clearly exceeds the 95% confidence limit. The zero hypothesis of a first order autoregressive process generating the signal can be rejected. The time series of the second PC of the zonal mean zonal wind (Fig. 5) does not show a distinctive low frequency oscillation. The peaks are of smaller amplitude and they occur more frequently. The power spectrum calculation of the second PC's years 350 to 900 (Fig. 6) reveals white noise as the dominant oscillation mode. The pattern of the second EOF of the zonal mean zonal wind is thus not important for the secular variability of the model. Therefore the negative correlation between the PNJ and the STJ is the

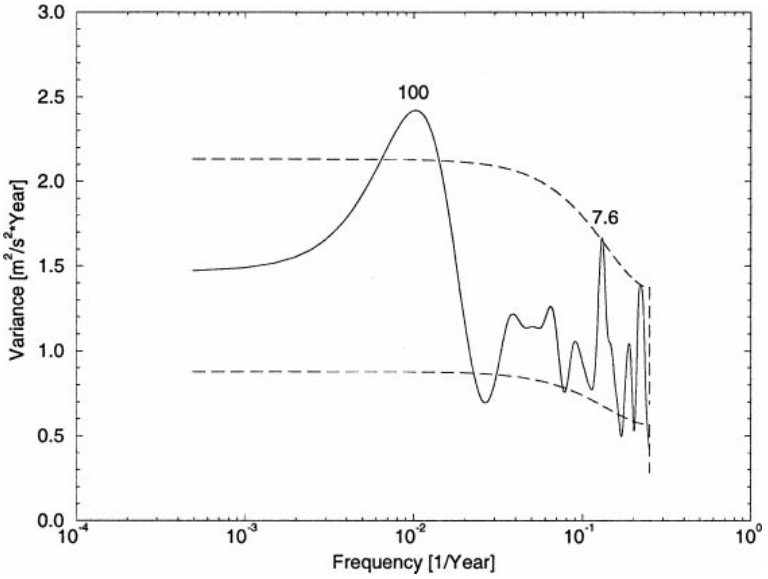

Fig. 4. Power spectrum of the first zonal mean zonal wind (control run, years 350–900) PC (Fig. 3). Variance is depicted against the logarithmic frequency [1/year]. The 95% confidence intervals of red noise are dashed. Significant periods [years] are marked

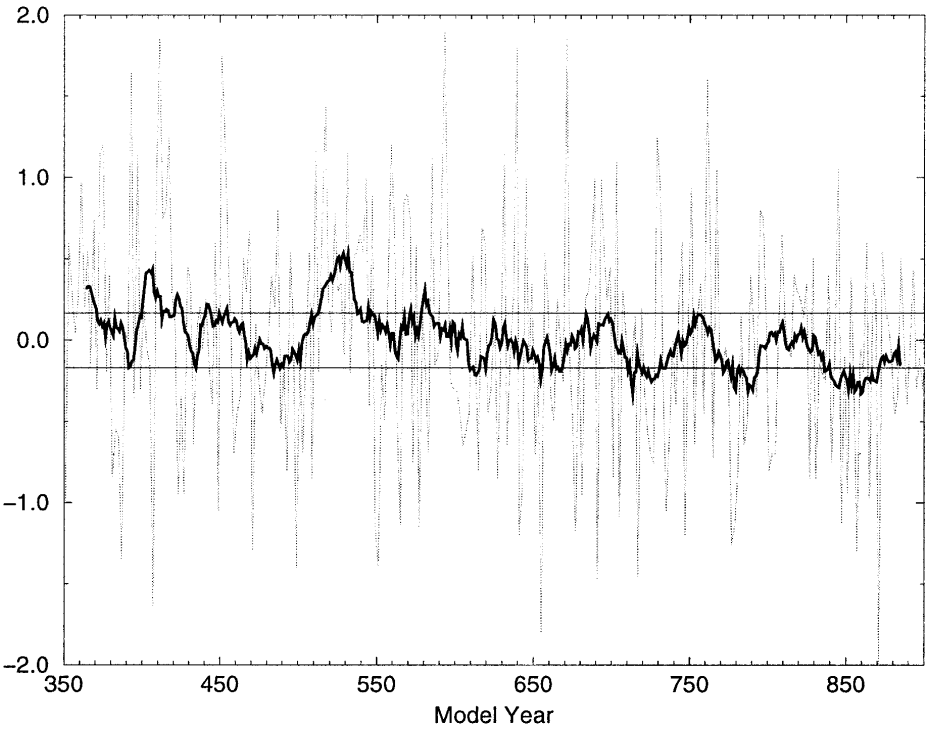

Fig. 5. Time series [years] of the second PC of winterly zonal mean zonal wind of the northern hemisphere (20° N–85.76° N; control run) smoothed with a two year running mean filter (grey line). The black line represents the 30 year running mean of the second PC's time series. Horizontal lines indicate one positive and one negative standard deviation of the smoothed time series

most important pattern for the long period variability in zonal wind. It is also a parameter for the strength of the polar vortex.

In order to examine the model variables involved in the oscillation a composite analysis is conducted. Therefore two zonal mean zonal wind regimes of the polar vortex are selected, one according to strong stratospheric zonal mean zonal wind, the other one to weak stratospheric zonal mean zonal wind. The two regimes are defined as years of large positive or negative amplitude of the first PC of zonal mean zonal wind, respectively. For the regime of anomalously strong (weak) zonal wind 30 year means greater (smaller) than one positive (negative) standard deviation of the first PC's time series smoothed by 30 year running means are chosen. Only the three maximum amplitudes of positive (negative) values between the years 350 and 900 are chosen. Since each point of the time series represents a mean of 30 years, 10 years around each chosen point are selected. Choosing 30

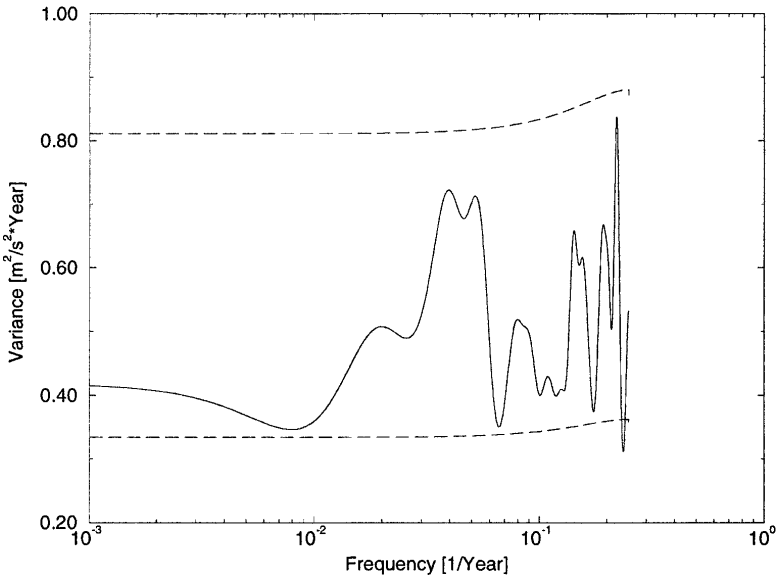

Fig. 6. Power spectrum of the second PC (Fig. 5) of zonal mean zonal wind (control run, years 350–900). Variance is depicted against the logarithmic frequency [1/year]. The 95% confidence intervals of blue noise are dashed. Significant periods [years] are marked

years around the time series point would lead to overlapping regions with years belonging both to the regime of anomalously strong and weak winds. About 100 years are selected representing each regime and for those years the composites are calculated for other model variables.

5. Composites of Geopotential Heights and Temperature

5.1 Geopotential Height

The examination of geopotential height shows the completely different circulation patterns of the two zonal mean zonal wind regimes. Composites of geopotential height anomalies for the two regimes were calculated both at the 50 and at the 500 hPa level.

The statistical significance of the composites is obtained using a decadal *t*-test. Therefore decadal means of the selected years for each regime are computed and used for the further calculation of the *t*-test. The test is calculated between the two composites of strong and weak zonal wind. Statistically significant differences between both regimes result. Regions of more than 95% statistical significance are shaded (see Fig. 7). Dark shading indicates positive values and light shading negative values. The patterns are not exactly linear, for this reason both composites are shown and not just their difference.

The most obvious feature of the geopotential height winter mean at the 50 hPa level is the symmetric polar stratospheric low-pressure system. During winter at high latitudes westerly winds dominate the stratosphere. The polar vortex is intensified for the regime of strong zonal wind (Fig. 7a). A weak positive geopotential height anomaly appears south of the Aleutian islands. This strengthens the southern part of the stratospheric Aleutian high. For the regime of weak zonal winds (Fig. 7b) the weakened polar vortex is the main feature.

The geopotential height winter mean at the 500 hPa level reveals the strong polar vortex. The geopotential height anomaly composite for the regime of anomalously strong zonal wind (Fig. 8a) displays a strengthened polar low-pressure system. The vortex centre is shifted towards the Atlantic. Geopotential height over the mid latitude North Pacific (between approximately 30 and 50° N) is 20 gpm above mean values, thereby weakening the southern flank of the Aleutian low, and strengthening slightly the Azores High. This and the negative anomalies over Iceland and Greenland contribute to an enhanced positive NAO index. The Aleutian Low is deepened at its southern edge for the regime of anomalously weak zonal winds (Fig. 8b). Negative geopotential height anomalies then can also be seen for the Azores High. The polar vortex is weakened. Only weak negative anomalies of the NAO index are typical for this phase. This is the result of positive geopotential height anomalies over Greenland and negative anomalies over the Azores High. These composites show the relation

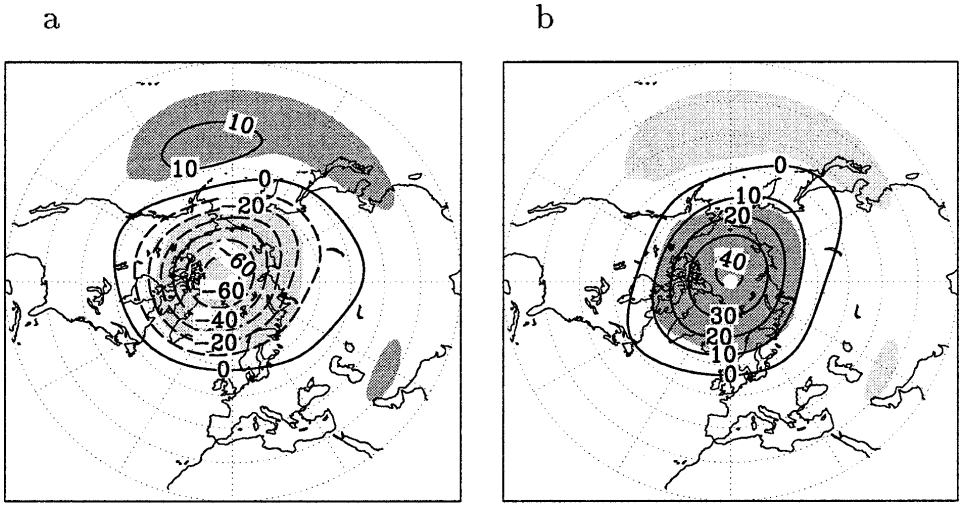

Fig. 7. Geopotential height anomaly ($\overline{DJF}$) composites [gpm] at the 50 hPa level for the regimes of strong (a) and weak (b) zonal mean zonal wind. Contour interval is 10 gpm. The northern hemisphere is shown from 20°N to 90° N. Shaded regions are statistically significant at the 95% level and higher, according to a decadal *t*-Test. Dark shaded regions indicate positive values and light shaded regions negative values, respectively

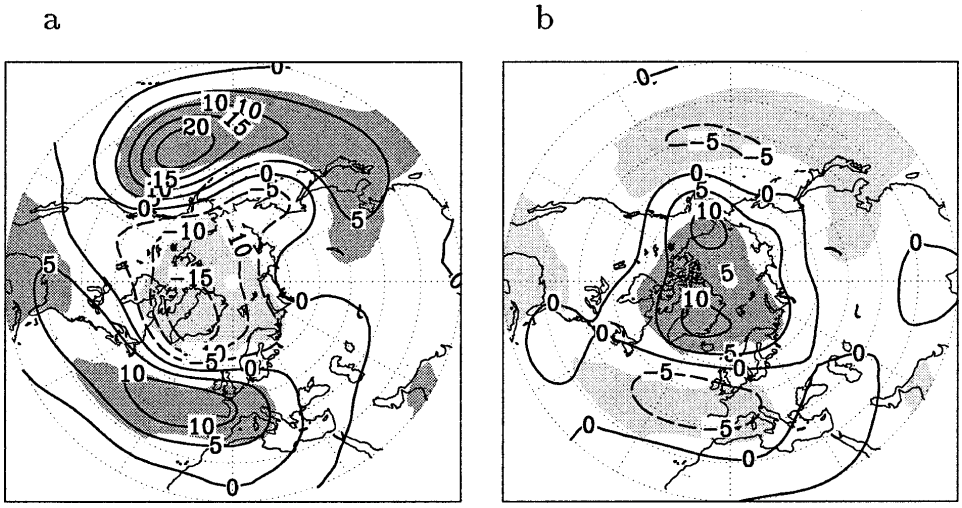

Fig. 8. Geopotential height anomaly ($\overline{DJF}$) composites [gpm] at the 500 hPa level for the regime of strong (a) and weak (b) zonal mean zonal wind. Contour interval is 5 gpm. The northern hemisphere is shown between 20° N and 90° N. Shaded regions: see Fig. 7

between the zonal mean zonal wind and the NAO. They show how the secular variability of the control run is mirrored by the NAO.

To understand the large differences between the two zonal wind regimes over the North Pacific, the region between 90° E and 90° W at the 500 hPa level is examined in more detail. During winter the centre of the low-pressure system is located over the Aleutian islands (Fig. 9) and high pressure can be seen over the western coast of northern America. For the regime of strong zonal wind (Fig. 9a) the south-eastern part of the Aleutian low is weakened substantially. This is caused by a spreading of high-pressure into the eastern Pacific. The south-eastern part of the Aleutian low is slightly strengthened for the regime of weak zonal wind (Fig. 9b). Positive anomalies can be seen to the north-east of the low-pressure system. The eastern Pacific subtropical high is slightly weakened. Figure 9c shows the difference of both composites and the maximum geopotential height variability at the 500 hPa level of 25 gpm over the south-eastern edge of the Aleutian low between both regimes of zonal mean zonal wind.

5.2 Near Surface Temperature

Regarding the consequences of the anthropogenic greenhouse effect the greatest attention is paid to the near surface temperature change. Together with such a temperature change the

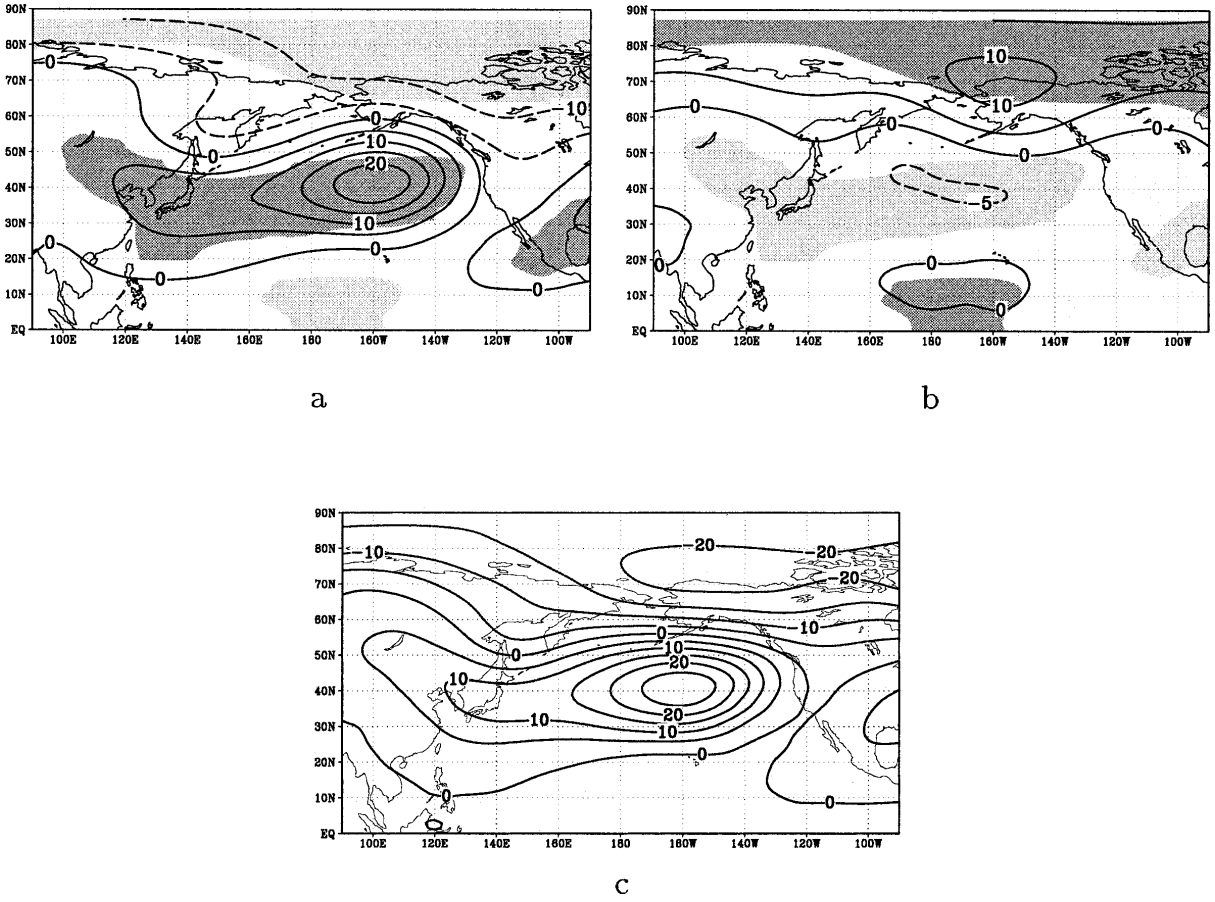

Fig. 9. Composites $(\overline{DJF})$ of geopotential height anomalies [gpm] at the 500 hPa-level for the regime of strong (a) and weak (b) zonal mean zonal wind. Shown is the Aleutian region between 0° N to 90° N and between 90° E and 90° W. Contour interval is 5 gpm. Shaded regions: see Fig. 7. Shown below (c) is the difference of both composites (a–b). Contour interval is 5 gpm

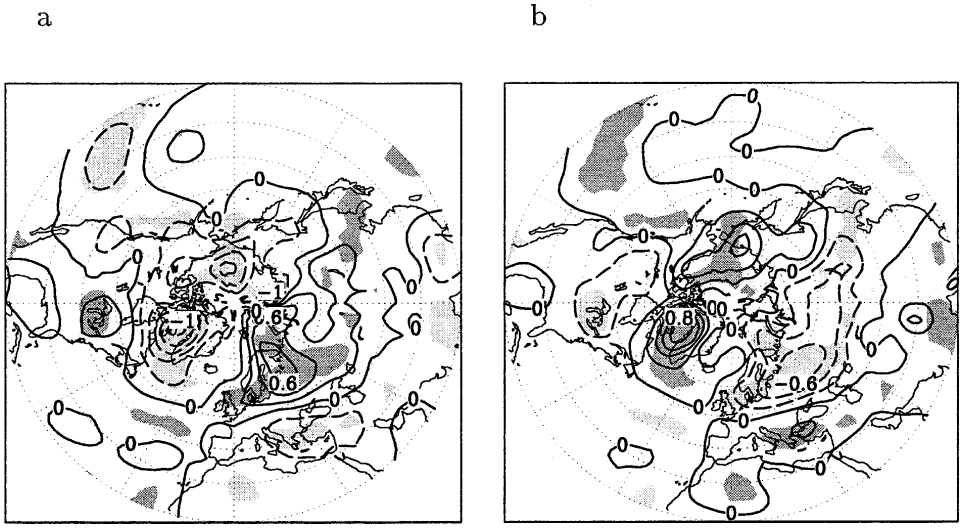

Fig. 10. Significant northern hemisphere winterly surface temperature anomalies [K] of the control run for the regime of strong (a) and weak (b) zonal mean zonal wind. Contour interval is 0.2 K. Shaded regions: see Fig. 7

humidity budget and precipitation can vary, and wind systems and planetary waves can be shifted. It is, therefore, important to know the temperature difference between significantly different regimes of the control run compared to the simulated greenhouse warming. The modeled variability must also be compared to observed temperature changes.

Significant near surface temperature anomalies ranging from -1 K to 0.6 K can be seen in the regime of strong zonal wind (Fig. 10a). The largest negative anomalies are located near

Greenland over the Davis Strait. The maximum positive anomalies are found in the eastern Baltic. The model depicts a pattern of positive values over the land surface and negative values over the ocean. This pattern is the expression of a favorite mode of the model (Perlwitz and Graf, in preparation). Wallace et al. (1996) attributed about 50% of the temperature changes observed in the recent decades to this dynamic mode.

For the regime of weak zonal wind (Fig. 10b) a similar temperature distribution with reversed signs can be seen. The extreme values lie between −0.6 K and 0.8 K. The largest positive temperature anomalies can be found over the Davis Strait and the largest negative anomalies are located over the western part of Russia and over Finland.

The near surface temperature changes are forced by advective processes. For the regime of anomalously strong zonal wind (Fig. 10a) the strengthened polar vortex forces an anomalous advection of warmer air towards northern Europe and of cooler polar air towards the Davis Strait. Positive anomalies of geopotential height south of the Aleutian Low advect polar air currents in the direction of the eastern Pacific. For anomalously weak zonal winds (Fig. 10b) a reverse advection pattern appears. These temperature changes can also be related to advective processes which are forced by geopotential height anomalies. The latter evolve from changes in phase and amplitude of ultra-long planetary waves due to different vertical propagation of planetary wave energy (Charney and Drazin, 1961; Perlwitz and Graf, 1995).

The increasing interest in anthropogenic influence on the climate system leads to the question to what degree the modeled temperature oscillation resembles the observed and simulated temperature trends of the last decades. For this comparison the observed winter near surface temperature data of Jones (1998) is used from 1958 to 1998 (Fig. 11). The mean temperature of years 1958 to 1967 was subtracted from the mean temperature of years 1989 to year 1998. The calculation reveals maximum temperature changes between − 2.7 K and 3.6 K. The largest negative trends are located over the Davis Strait. Positive trends are most pronounced over Russia.

An IPCC (1995) scenario A model run (Voss et al., 1998) is used for comparison of natural

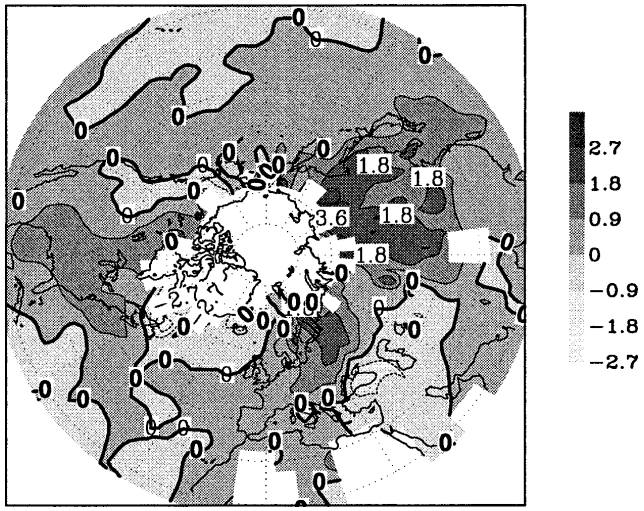

Fig. 11. Observed mean temperature of years 1958 to 1967 minus mean temperature of years 1989 to 1998. Contour interval is 0.9 K

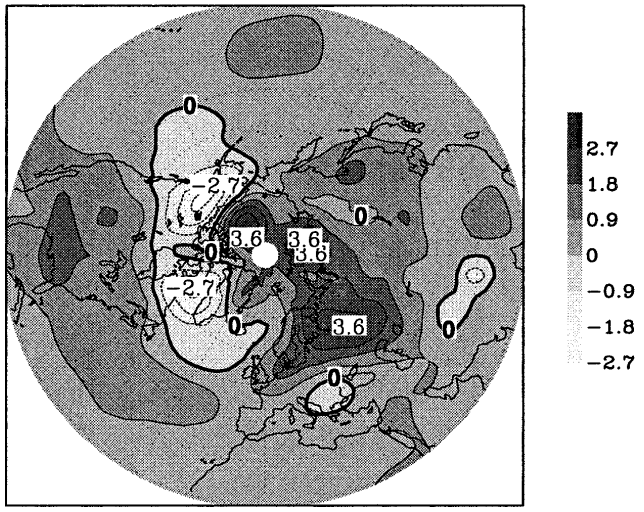

Fig. 12. According to IPCC scenario A modeled winterly temperature changes between years 1958 to 1967 and years 1989 to 1998. Contour interval is 0.9 K

variability with simulated anthropogenically forced trends (Fig. 12). The simulation starts at the model year 149 of the control run with the near pre-industrial CO_2 level of 1880. The difference between years 1989 to 1998 and years 1958 to 1967 shows maximum temperature changes of − 2.7 K to 3.6 K. The maximum negative temperature trends are located over the Davis Strait and over Alaska, positive trends are at a maximum over the coast of northernmost Russia to the Barent Sea and over the western part of Russia.

The difference between the near surface temperature composites of both zonal wind regimes (Fig. 10) reveals the maximum control run variability. The temperature trends range from − 1.8 K over the Davis Strait to 1.2 K over Estonia.

For the observed and the two modeled data sets the regions of cooling are very similar. The strongest cooling trends are found over the Davis Strait in all three temperature trend graphics. The warming regions are located at somewhat different places in the three data sets, but the warming tendency over the land surface can be seen in all of them. Especially the two simulated trends show many similarities in the location of the warmest and coolest trends. This implies that the variation of the control run temperature is part of the modeled warming scenario, i.e. the forced climate variation is not orthogonal to the natural variability. An important amount, though not all, of the scenario's simulated temperature changes can be explained by the natural variations of the control run. Therefore these must not be neglected in the climate change scenario computations. The control run variability resembles sufficiently well the observed temperature trend pattern, indicating that the observed trends might possibly be due to an enhanced natural variability mode. In this case, the model has to be brought in phase with natural variability before starting the scenario calculations in order to prevent getting modified results due to an underlying trend that is not in phase with natural variations. This could be done by carefully investigating the long-term variability of parameters involved in the here described variability mode both in observations and in the model. The start point of a model simulation may then be determined by matching the history of observations and model for at least one cycle of the multi-decadal variability. Performing the usual ensemble of few independent simulations around this starting point would then provide an optimal coverage of the sub-phase space of climate.

6. Chaotic Behavior of the Oscillation Frequencies

The time series of the first PC of the zonal mean zonal wind (Fig. 3) shows no trend and remains stable with time. After the year 1000 the oscillation amplitude becomes distinctively smaller. The period of the variability seems to be shorter, too. For a closer examination of this feature a fourier filter is applied to the time series. The bandpass filter is applied for the range of 15 to 35 years and for 70 to 110 years. The standard deviation of the fourier filtered time series is calculated and smoothed using a running average of 500 years (Fig. 13). Long periods

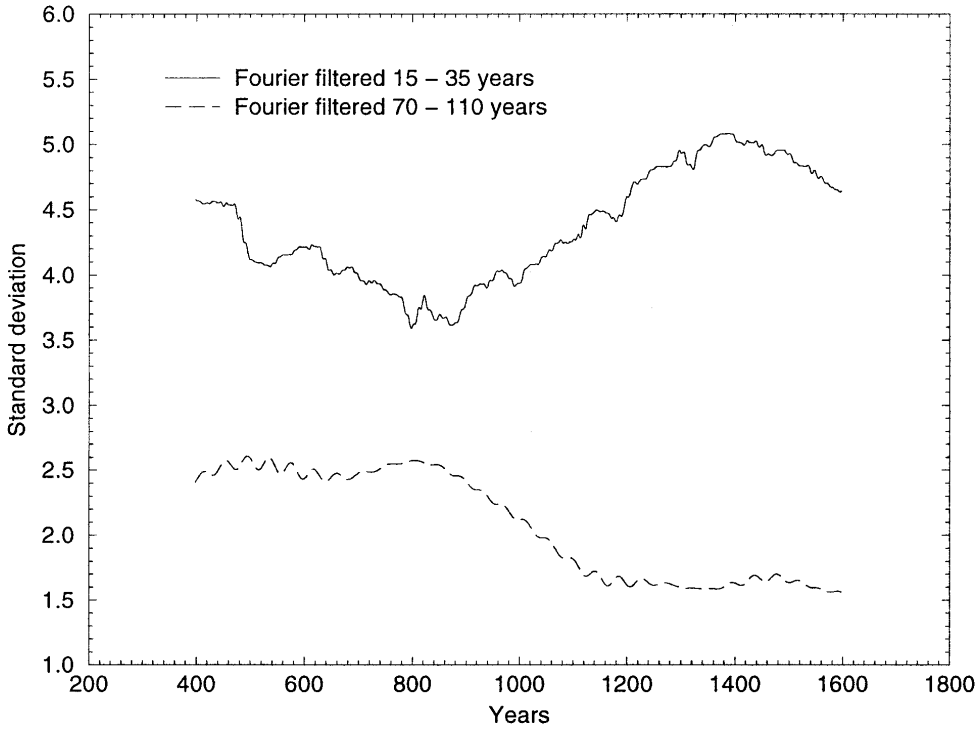

Fig. 13. 500 year running average of the standard deviation of the fourier filtered principal component of northern hemisphere winterly zonal mean zonal wind (20° N–85.76° N). Bandpass filtered for the 70–110 year (stippled) and 15–35 year interval (solid line)

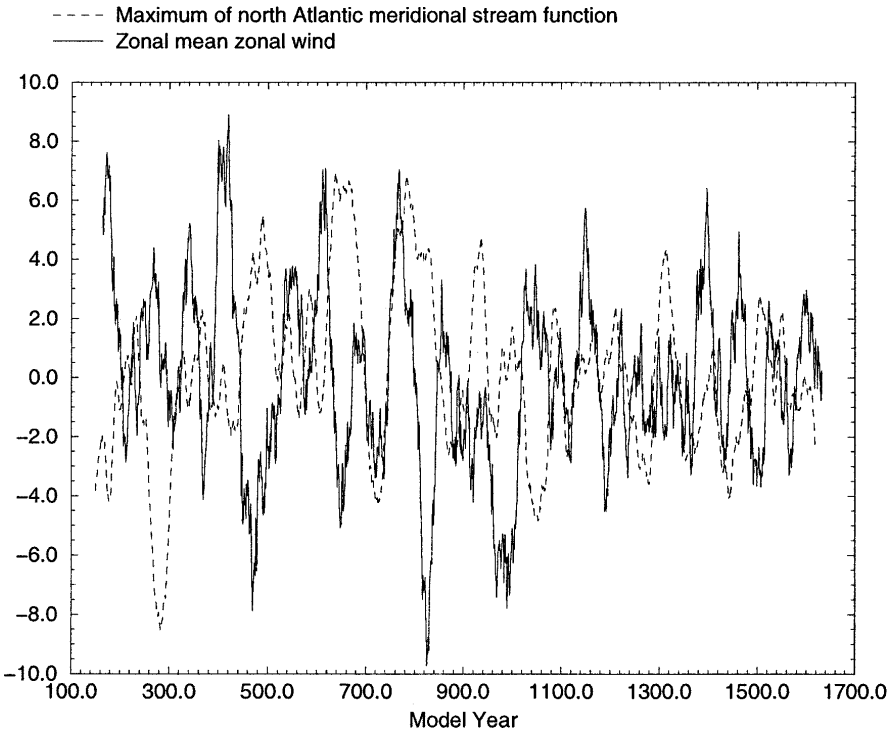

Fig. 14. First principal component of northern hemisphere (20° N–85.76° N) winterly zonal mean zonal wind (solid line) of the control run and maximum of meridional stream function (stippled) of the LSG-model in the northern atlantic (see Fig. 6 of (Timmermann et al., 1998)). Both time series are smoothed with a 30 year running mean filter

have a nearly constant portion of total variability up to the year 900. After that the influence of low frequency variability decreases and the shorter periods become increasingly important.

A possible forcing of low frequency variability is the thermohaline circulation of the oceans. The North Atlantic is extremely important in this context because this is where deep water formation takes place. To study changes in deep water formation in the North Atlantic the calculations of Timmermann et al. (1998) (see their Fig. 6) are used. The maximum of the North Atlantic meridional stream function was computed and the time series of the maximum is shown in Fig. 14. This index was also used by Delworth et al. (1993). Like the time series of zonal mean zonal wind the thermohaline circulation is also stable and shows no significant trend. The period of the variation of the meridional circulation is approximately 135 years. Shorter periods after the year 1000 can also be seen in the ocean. The periods do not fit well with those of the atmosphere. Timmermann (1998) defined a sea level pressure index as the pressure averaged between 30° W and 34° W and between 70° N and 80° N. The time series of this index (Fig. 15) shows multi-decadal variability for the first 1000 years. From year 1050 to year 1500 shorter oscillation modes can be seen as for the zonal mean zonal wind time series. But in contrast to the zonal wind time series the short frequency vacillations are superposed by secular variabilities with periods of more than 200 years. After the year 1600 a peak of large amplitude of an underlying lower frequency oscillation can be seen. This can be an indication of a transition towards lower frequency variability such as the one that appears between the years 850 and 1050. Ice core examinations have revealed sudden climate shifts in between and after the last ice ages for the North Atlantic region. Manabe and Stouffer (1995) simulated a thermohaline circulation collapse in their coupled atmosphere-ocean model by introducing large quantities of fresh-water into the North Atlantic. Weaver and Sarachnik (1991) showed with their GCM an oscillation between deep water formation and collapsed thermohaline circulation. The oscillation period is of decadal time-scale, dominated by advective processes.

The transition between different periods of the zonal mean zonal wind time series (Fig. 13) as well as of the SLP time series (Fig. 15) indicates that chaotic processes within the atmosphere-ocean system might be involved. Firstly the ultra-long periods remain stable for a certain time interval before a sudden regime shift occurs, leading to a prevalence of shorter periods.

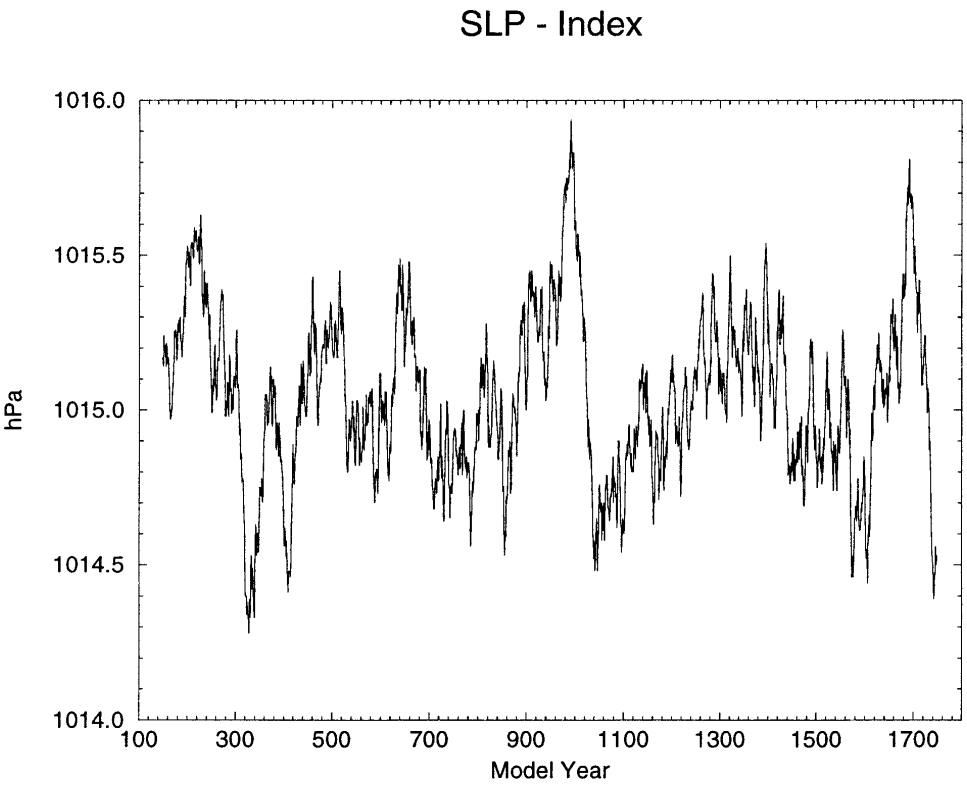

Fig. 15. Sea level pressure [hPa] of the ECHAM3/LSG-model in the vicinity of Greenland for 1600 years of the control run (Timmermann, 1998). Pressure is averaged between 30° W and 34° W and between 70° N and 80° N. The time series is smoothed with a 50 year running mean filter

According to our thesis of a chaotic time series, we suggest that the thermohaline circulation is not a forcing for the secular variability of the zonal mean zonal wind but rather a result of the chaotic processes occurring within the modeled atmosphere-ocean system. Basically the secular variability of the model is characterized by chaotic structures with included trends of the model's variables. The zonal mean zonal wind time series has several segments of stable regimes. During those segments climate predictability is greatly enhanced. But it is impossible to predict the first appearance of these segments or how long they will last because of the chaotic structure of the time series.

7. Conclusions

The secular variability of the modeled ECHAM3/LSG coupled tropospheric and strato-spheric circulation is analyzed in this paper. We use the first EOF of zonal mean zonal wind, which describes a negative correlation between the PNJ and the STJ, as a diagnostic parameter. Regimes of anomalously strong and anomalously weak zonal wind are selected using zonal wind values greater than one positive and smaller than one negative standard deviation of the zonal mean zonal wind's first PC time series. For these years composites with other model variables are calculated. Secular variability is identified for the strength of the polar vortex and the position of the Aleutian Low with this method. The NAO index attains positive anomalies during the regime of anomalously strong zonal wind, and negative anomalies for the weak zonal wind composites.

A comparison between observed temperature trends of the last decades and internal model temperature variability, as well as temperature trends of a climate change scenario computed with the model, reveal that the control run variations can possibly explain a large part of the observed and simulated trends. If we take into account that there exist some data gaps in the observations, in example over the Arctic, we can say that the locations of the warming and especially the cooling regions are in quite good agreement for the three trend patterns. Even though there are some exceptions like an observed warming region over Canada which can not be seen in the models and a large warming trend over Siberia in the scenario run which can not be detected in the control run, these results show the necessity of bringing the internal vacillations of the model in phase with

natural variability to avoid a superimposition of trends.

The time series of zonal mean zonal wind shows a shift in period towards shorter time scales. After the year 1000 the secular oscillations become less important compared to the inter-decadal variations which dominate the whole time series, especially during the second half of the time series. A comparison with a SLP time series leads to the suggestion of a regime shift because after the year 1600 the large amplitudes and lower frequencies reappear. The secular variability of the model has chaotic character and is therefore not predictable. Shorter segments of the time series include trends of the model's variables and stable regimes. During those segments a more accurate climate predictability is possible. The occurrence of these stable modes is not predictable because of the chaotic behavior of the time series.

Further studies with different coupled atmosphere-ocean GCMs concerning secular variability are necessary. Comparisons of the modeled variations with observed trends would lead to a better understanding of natural low frequency variability modes. Time series of ice cores are well suited for this purpose. A better knowledge of the current secular oscillation state could lead to a more accurate estimate of the natural climate condition.

Acknowledgements

We would like to thank R. Voss for supplying the ECHAM3/LSG control run and his help in obtaining the LSG data. A. Timmermann provided the time series of maximum meridional overturning and the SLP as well as many helpful ideas and comments. A. Bacher prepared the power spectrum program and contributed useful suggestions. Helpful comments of I. Kirchner and the two anonymous reviewers are gratefully acknowledged. This work was supported by the Bundesministerium für Bildung, Wissenschaft, Forschung und Technologie (BMBF, Germany) grant 01 L09512/0 (Ozone Research Program).

References

Appenzeller, C., Schwander, J., Sommer, S., Stocker, T. F., 1998: The North Atlantic Oscillation and its imprint on precipitation and ice accumulation in Greenland. *Geophys. Res. Lett.,* **25**(11), 1939–1942.

Appenzeller, C., Stocker, T. F., Anklin, M., 1998: North Atlantic Oscillation Dynamics Recorded in Greenland Ice Cores. *Science,* **282**(16), 446–449.

Charney, J. G., Drazin, P. G., 1961: Propagation of planetary-scale disturbances from the lower into the upper atmosphere. *J. Geophys. Res.,* **66**, 83–109.

Cubasch, U., Santer, B. D., Hellbach, A., Hegerl, G., Höck, H., Maier-Reimer, E., Mikolajewicz, U., Stössel, A., Voss, R., 1994: Monte Carlo climate change forecasts with a global coupled ocean-atmosphere model. *Clim. Dyn.,* **10**, 1–19.

Dansgaard, W., Johnson, S. J., Clausen, H. B., Langway, C. C., 1970: Climatic record revealed by the Camp Century Ice Core. In: Turekian, K. K. (ed.) *The Late Cenozoic Glacial Ages*. Yale, New Haven, pp. 37–56.

Delworth, T. L., Manabe, S., Stouffer, R. J., 1993: Interdecadal variations of the thermohaline circulation in a coupled ocean-atmosphere model. *J. Climate,* **6**(11), 1993–2011.

Deutsches Klimarechenzentrum, Modellbetreuungsgruppe, 1992: The Hamburg Large Scale Geostrophic Ocean General Circulation Model, Technical Report No. 2. Revision 1.

Deutsches Klimarechenzentrum, Modellbetreuungsgruppe, 1994: The ECHAM3 Atmospheric General Circulation Model, Technical Report No. 6. Revision 3.

Gajewski, K., 1988: Late holocene climate changes in Eastern North America estimated from pollen data. *Quat. Res.,* **29**, 255–262.

Graf, H.-F., Kirchner, I., Perlwitz, J., 1998: Changing lower stratospheric circulation: The role of ozone and greenhouse gases. *J. Geophys. Res.,* **103**(D10), 11, 251–11,261.

Graf, H.-F., Perlwitz, J., Kirchner, I., 1997: Coupled modes of tropospheric and stratospheric circulation in nature and in models. In: Stratospheric Processes and their role in Climate (SPARC), Vol. 1 of *World Climate Research Programme*, International Council of Scientific Unions, Intergovernmental Oceanographic Commission, World Meteorological Organization, WMO, pp. 129–132.

Hegerl, G. C., Hasselmann, K., Cubasch, U., Mitchell, J. F. B., Roeckner, E., Voss, R., Waszkewitz, J., 1997: Multi-fingerprint detection and attribution analysis of greenhouse gas, greenhouse gas-plus-aerosol and solar forced climate change. *Clim. Dyn.,* **13**, 613–634.

Houghton, J. T., Jenkins, G. J., Ephraums, J. J., 1990: *Climate Change*. *The IPCC Scientific Assessment.* Cambridge: Cambridge University Press.

Johnson, S. J., Dansgaard, W., Clausen, H. B., Langway, C. C., 1970: Climatic Oscillations 1200–2000 a.d. *Nature,* **227**, 482–483.

Jones, P. D., 1998: http://ingrid.ldgo.columbia.edu/SOURCES/.UEA/.CRU/.Jones/.landsea/.

Kodera, K., Koide, H., 1997: Spatial and seasonal characteristics of recent decadal trends in the Northern Hemispheric troposphere and stratosphere. *J. Geophys. Res.,* **102**(D16), 19433–19447.

Kodera, K., Chiba, M., Yamazaki, K., Shibata, K., 1991: A possible influence of the polar night stratospheric jet on the subtropical tropospheric jet. *J. Meteor. Soc., Japan*, **69**(6), 715–721.

LaMarche, V. R., 1974: Paleoclimatic inferences from long tree-ring records. *Science*, **183**, 1043–1048.

Lamb, H. H., 1977: *Climate: Present*, *Past and Future*, Vol. 2. London: Methuen.

Maier-Reimer, E., Mikolajewicz, U., Hasselmann, K., 1993: Mean circulation of the Hamburg LSG OGCM and its sensitivity to the thermohaline surface forcing. *J. Phys. Oceanogr.,* **23**, 731–757.

Manabe, S., Spelman, M. J., Bryan, K., 1991: Transient response of a coupled ocean-atmosphere model to gradual changes of atmospheric CO_2. Part I: Annual mean response. *J. Climate,* **4**, 785–818.

Manabe, S., Stouffer, R. J., 1995: Simulation of abrupt climate change induced by freshwater input to the North Atlantic Ocean. *Nature,* **378**, 165–167.

Manley, G., 1974: Central England temperatures: monthly means 1659–1973. *Quart. J. Roy. Meteor. Soc.,* **100**, 389–405.

Nigam, S., 1990: On the structure of variability of the observed tropospheric and stratospheric zonal-mean zonal wind. *J. Atmos. Sci.,* **47**(14), 1799–1813.

Perlwitz, J., Graf, H.-F., 1995: The statistical connection between tropospheric and stratospheric circulation of the northern hemisphere in winter. *J. Climate,* **8**(10), 2281–2295.

Perlwitz, J., Graf, H.-F., Kirchner, I., 1995: Increasing greenhouse effect and ozone trends. In: Stratospheric Processes and their role in Climate (SPARC), Vol. 2 of *World Climate Research Programme*, International Council of Scientific Unions, Intergovernmental Oceanographic Commission, World Meteorological Organization, WMO, pp. 461–464.

Perlwitz, J., Graf, H.-F., Voss, R., n.d.: The leading mode of the coupled troposphere-stratosphere winter circulation in different climate regimes. *J. Geophys. Res.* (submitted).

Roeckner, E., Arpe, K., Bengtsson, L., Brinkop, S., Dümnil, L., Esch, M., Kirk, E., Lunkeit, F., Ponater, M., Rockel, B., Sausen, R., Schlese, U., Schubert, S., Windelband, M., 1992: Simulation of the present-day climate with the ECHAM model: Impact of model physics and resolution. MPI Report No. 93, 172 pages.

Schiller, A., Mikolajewicz, U., Voss, R., 1996: The stability of the thermohaline circulation in a coupled ocean-atmosphere general circulation model. Max-Planck-Institute for Meteorology. Reports, No. 188, 42 p.

Schönwiese, C. D., 1978: Central England temperature and sunspot variability 1660–1975. *Arch. Met. Geoph. Biocl.,* **B26**, 1–16.

Stuiver, M., Braziunas, T. F., 1989: Atmospheric ^{14}C and century-scale solar oscillations. *Nature*, **338**, 405–408.

Tett, S. F. B., Johns, T. C., Mitchell, J. F. B., 1997: Global and regional variability in a coupled AOGCM. *Clim. Dyn.,* **13**, 303–323.

Thompson, D. W. J., Wallace, J. M., 1998: The Arctic Oscillation signature in the wintertime geopotential height and temperature fields. *Geophys. Res. Lett.,* **25**(9), 1297–1300.

Timmermann, A., 1998: Personal communications.

Timmermann, A., Latif, M., Voss, R., Grötzner, A., 1998: Northern hemispheric interdecadal variability: a coupled air-sea mode. *J. Climate,* **11**, 1906–1931.

Voss, R., Sausen, R., Cubasch, U., 1998: Periodically synchronously coupled integrations with the atmosphere-ocean general circulation model ECHAM3/LSG. *Clim. Dyn.,* **14**, 249–266.

Wallace, J. M., Zhang, Y., Bajuk, L., 1996: Interpretation of interdecadal trends in northern hemisphere surface air temperature. *J. Climate,* **9**, 249–259.

Weaver, A. J., Sarachnik, E. S., 1991: Evidence for decadal variability in an ocean general circulation model: an advective mechanism. *Atmos.-Ocean,* **29**(2), 197–231.

Authors' addresses: Frauke Feser, Meteorological Institute of the University of Hamburg, Germany; Hans-F. Graf and Judith Perlwitz, Max-Planck-Institute for Meteorology, Bundesstrasse 55, D-20146 Hamburg, Germany.